Science of the Total Environment 903 (2023) 166607

Contents lists available at ScienceDirect

Science of the Total Environment

journal homepage: www.elsevier.com/locate/scitotenv

Detection and attribution of the start of the growing season changes in the Northern Hemisphere

Haihua Chen, Jianjun Zhao *, Hongyan Zhang *, Zhengxiang Zhang, Xiaoyi Guo, Meiyu Wang

Key Laboratory of Geographical Processes and Ecological Security in Changbai Mountains, Ministry of Education, School of Geographical Sciences, Northeast Normal University, Changchun 130024, China
Urban Remote Sensing Application Innovation Center, School of Geographical Sciences, Northeast Normal University, Changchun 130024, China

HIGHLIGHTS

- The start of the growing season (SOS) is significantly advanced in 1982–2015.
- The SOS is most sensitive to changes in temperature, humidity and frost frequency.
- Increased temperature and humidity can advance the SOS.
- Increased frost can delay the SOS.

GRAPHICAL ABSTRACT

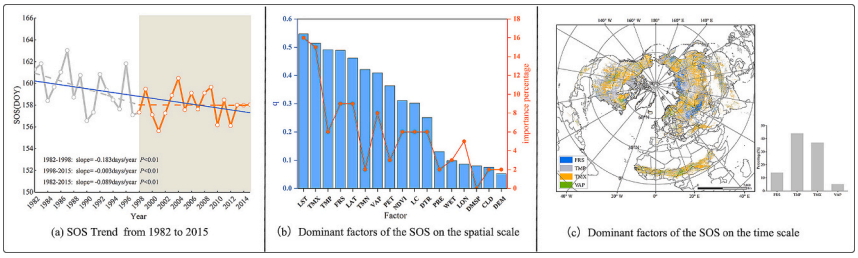

ARTICLE INFO

Editor: Elena Paoletti

Keywords:
Vegetation phenology
The start of the growing season (SOS)
GIMMS3g
Northern Hemisphere

ABSTRACT

Global climate change has led to significant changes in land surface phenology. At present, research on the factors influencing the start of the growing season (SOS) mainly focuses on single factor effects, such as temperature and precipitation, ignoring the combined action of multiple factors. The impact of multiple factors on the spatial and temporal patterns of the SOS in the Northern Hemisphere is not clear, and it is necessary to combine multiple factors to quantify the degrees of influence of different factors on the SOS. Based on the GIMMS3g NDVI dataset, CRU climate data and other factor data, we used geographic detector model, random forest regression model, multiple linear regression, partial correlation analysis and Sen + Mann-Kendall trend analysis to explore the variation of the SOS in the Northern Hemisphere to reveal the main driving factors and impact threshold of 17 influencing factors on the SOS. The results showed that (1) during the past 34 years (1982–2015), the SOS in Europe and Asia mainly showed an advancing trend, whereas the SOS in North America mainly showed a delaying trend. (2) The SOS was mainly controlled by frost frequency, temperature and humidity. Increasing frost frequency inhibited the advancement of the SOS, and increasing temperature and humidity promoted the advancement of the SOS. (3) There were thresholds for the influences of the driving factors on the SOS. Outside the threshold ranges, the response mechanism of the SOS to driving factors changed. The results are important for understanding the response of the SOS to global climate change.

* Corresponding authors at: Key Laboratory of Geographical Processes and Ecological Security in Changbai Mountains, Ministry of Education, School of Geographical Sciences, Northeast Normal University, Changchun 130024, China.
E-mail addresses: zhaojj662@nenu.edu.cn (J. Zhao), zhy@nenu.edu.cn (H. Zhang).

https://doi.org/10.1016/j.scitotenv.2023.166607
Received 7 July 2023; Received in revised form 10 August 2023; Accepted 25 August 2023
Available online 27 August 2023

1. Introduction

Global warming and extreme weather events are occurring far more frequently than people previously expected (IPCC, 2018). Vegetation adapts to global climate change by regulating its own phenological events (Zhang et al., 2020), and in turn, vegetation influences the exchange of energy, water and carbon between the land surface and the atmosphere, thereby regulating climate change (Peñuelas et al., 2009; Piao et al., 2008; Richardson et al., 2010). Studies have shown that rising spring temperatures in recent decades have led to a significant advance in the start of the growing season (SOS) in the Northern Hemisphere (Fu et al., 2016; Piao et al., 2015), which in turn has affected the balance of water, carbon and nutrients on land (Keenan et al., 2014; Peñuelas et al., 2009). Changes in phenology profoundly affect the structure and function of ecosystems (Fu et al., 2020) and make important contributions to understanding how ecosystems respond to changing environments.

Many scholars have carried out studies on vegetation phenology, which can be traced back to the ancient agricultural era (Piao et al., 2019). Traditional vegetation phenology monitoring is mainly field monitoring, which is time-consuming and labor-intensive with a limited observation range (Zhao et al., 2015). With the rapid development of remote sensing technology, vegetation phenology monitoring has gradually reached a mature stage (Piao et al., 2019). From the rich remote sensing data products to the extraction of phenological parameters from the products, a relatively systematic parameter extraction scheme has been formed. Extracting phenological parameters from remote sensing data mainly includes three steps, namely, constructing a time series dataset, fitting a vegetation index time series curve and extracting phenological parameters (Piao et al., 2019). Different data sources and parameter extraction methods have their own advantages and disadvantages, and scholars choose the optimal data source and method according to the research problem.

In recent decades, scholars have conducted deeper research on the trend changes in the SOS at different temporal and spatial scales. The research showed that the SOS advanced significantly in the Northern Hemisphere in the late 20th century, advancing by 0.34 days per year, while the trend of advancement of the SOS slowed down significantly in the early 21st century, advancing by only 0.02 days per year (Wang et al., 2019b). The variation range and trend of the SOS at the global, hemispheric, intercontinental and regional scales were not uniform, the advance time varied, and there was a phenomenon of reversal in some regions (Piao et al., 2019, 2006; Zhao et al., 2015). Vegetation is very sensitive to climate change (Jeong et al., 2011). The initial growth stage of vegetation is mainly controlled by temperature, photoperiod and winter cold (Körner and Basler, 2010). Temperature, precipitation and photoperiod are generally considered to be the main factors controlling the SOS (Fu et al., 2020; Piao et al., 2019). The response relationship between the SOS and driving factors varies from region to region, generally showing that when temperature increases, the SOS advances (Wang et al., 2019b) and that when precipitation increases, the SOS advances (Tao et al., 2017). Research has shown that since 1971, the SOS has advanced 2.5 days for every 1° increase in global annual average temperature (Körner and Basler, 2010). Photoperiod plays a secondary role in the SOS and mediates the SOS mainly by interacting with other environmental factors (Fu et al., 2020). In addition, winter chilling (Song et al., 2020), land cover types (Deng et al., 2019), latitude (Shen et al., 2015), nutrients (De Barba et al., 2016), elevation (Meng et al., 2021), near-surface temperature maximum (Piao et al., 2015) and atmospheric CO_2 concentration all have an impact on the SOS, even more so than hydrothermal conditions. The intensification of human activities has changed the developmental environment of vegetation, which makes an important contribution to the change in SOS (Fan et al., 2019). In general, the dominant influencing factors of the SOS have been studied from different perspectives, such as different data sources, different time ranges, and different research areas. However, with the increase in research on the correlation between the SOS and influencing factors, the driving factors of the SOS are becoming increasingly diverse. Collecting the influencing factors that have been proposed, the driving factors of the SOS mainly belong to climatic conditions, human activities, geographical location and vegetation types. Among the many influencing factors that have been proposed by scholars, which one is the most dominant, whether the dominant influencing factors of the SOS obtained from the two dimensions of time and space are consistent, and whether the recognized temperature and precipitation are still the most favorable indicators to explain the temporal and spatial variation in the SOS remain to be explored. This research provided a comprehensive picture of the relationship between environmental factors and the SOS in the Northern Hemisphere, which is helpful for understanding the development dynamics of the SOS more comprehensively and projecting the SOS changes.

Global climate change has led to the variations of the SOS in the Northern Hemisphere, but the main drivers affecting its spatial differentiation and interannual variability remain unclear. Based on the random forest model, geographic detectors and multiple linear regression, this research quantitatively analyzes the impacts of geographic location, climate change and human activities on the SOS in the Northern Hemisphere from both temporal and spatial scales and reveals the dominant factors affecting the SOS. The main objectives of this research were to 1) reveal the temporal and spatial variations in the SOS at the hemispheric scale; 2) explore the influence of different factors on the variation in the SOS in the Northern Hemisphere and quantify the dominant driving factors of the SOS; and 3) reveal the impact thresholds of major driving factors and clarify the pattern of interactions between the SOS and the dominant factors.

2. Data and methods

2.1. Data

2.1.1. GIMMS3g NDVI dataset

The third-generation Global Inventory Monitoring and Modeling Study (GIMMS) group of NDVI data was used in this research. The dataset has a spatial resolution of 8 km and a temporal resolution of 15 days. We used these remote sensing data to extract the SOS.

2.1.2. CRU dataset

The climate data adopt the CRU dataset. The dataset includes cloud cover (CLD), diurnal temperature range (DTR), ground frost frequency (FRS), near-surface temperature (TMP), near-surface temperature maximum (TMX), near-surface temperature minimum (TMN), potential evapotranspiration (PET), precipitation (PRE), vapor pressure (VAP) and wet day frequency (WET).

2.1.3. MODIS land cover dataset

The land cover data used the MCD12C1 dataset product. This research used the 2001–2015 dataset products to extract land cover types that remained unchanged from 2001 to 2015.

2.1.4. DMSP/OLS NTL data

The Defense Meteorological Satellite Program/Operational Linescan System (DMSP/OLS) night-time stable light (NTL) dataset came from the National Geophysical Data Center (NGDC) under the National Oceanic and Atmospheric Administration (NOAA), with a spatial resolution of 0.008333° and a temporal length of 1992–2013.

2.1.5. Other dataset

We used the DEM dataset and MODIS MYD11A2 land surface temperature (LST) dataset. Detailed introductory information on the data can be found in Table 1.

Table 1
The data used in this paper.

Name	Resolution	Time	Link
GIMMS3g NDVI	8 km	1982–2015	http://glcf.umd.edu/data/gimms/
CRU	0.5°	1982–2015	https://catalogue.ceda.ac.uk/
MCD12C1	0.05°	2001–2015	https://lpdaac.usgs.gov/products/mcd12c1v006/
DEM	0.08333°		http://www.fao.org/soils-portal/soil-survey/soil-maps-and-databases/harmonized-world-soil-database-v12/en/
Night-Time Stable Light (NTL)	0.008333°	1992–2013	https://ngdc.noaa.gov/eog/dmsp/
Land Surface Temperature (LST)	0.05°	2000–2015	https://ladsweb.modaps.eosdis.nasa.gov/missions-and measurements/products/MYD11A2/

2.2. Methods

2.2.1. SOS extraction

In this research, missing values in the GIMMS3g NDVI dataset were filled. The SG (Savitzky and Golay, 1964) filtering method was used to coarsely fit the long-term NDVI data series.

Based on AG fitting (Jonsson and Eklundh, 2002), the long-term NDVI data were finely fitted, and the phenological parameters were extracted by the threshold method (Fischer, 1994; White et al., 1997) (the threshold was set to 0.2–0.6) and the derivative method (Piao et al., 2006; Studer et al., 2007). Based on the DL (Beck et al., 2006), Elmore Double Logistic (Elmore et al., 2012) and Piecewise Logistic function (Zhang et al., 2003) models, the long-term NDVI data were finely fitted, and the phenological parameters were extracted by the derivative method (Piao et al., 2006; Studer et al., 2007). Based on the Harmonic Analysis of Time Series (HANTS) (Roerink et al., 2000) and spline methods (Craven and Wahba, 1979; Friedman and Roosen, 1995), the long-term NDVI data were finely fitted, and the phenological parameters were extracted by the midpoint method (Delbart et al., 2005; White et al., 1997). The average of the 11 phenological parameter data obtained by the above 6 fitting models and 3 extraction methods was taken as the SOS of the Northern Hemisphere.

Based on MODIS land cover data from 2000 to 2015, the SOS was extracted for regions where the vegetation type remained constant. We excluded pixels with NDVI < 0.1 (Shen et al., 2014), removing the effect of sparsely vegetated regions from the results. We also removed regions with a seasonality >1. To reduce the interference of other factors, the pixels with SOS variation coefficients >15 were removed. Finally, the above masked data were used as the data in this research (Fig. S1).

2.2.2. Sen + Mann–Kendall trend analysis

We used the Theil–Sen (TS) slope and the Mann–Kendall (MK) test to calculate the trend of significance of the SOS in the Northern Hemisphere over 34 years ($P < 0.05$). TS is a robust nonparametric statistical trend calculation method with the slope calculated as (Mann, 1945):

$$Q = median\frac{Xj - Xi}{j - i}\ 1 < i < j < n \tag{1}$$

Q is the TS slope, and xj and xi are the series values at moments j and i. A Q value >0 indicates an upward trend, and a Q value <0 indicates a downward trend.

The Mann–Kendall test was used to assess the significance of trend changes in the time series data (Farlie and Kendall, 1971), and the Mann–Kendall test procedure was as follows:

$$\tau = \sum_{i=1}^{n-1}\sum_{j=i+1}^{n} sign(xj - xi), \text{且} \operatorname{sign}(xj - xi) = \begin{cases} 1\ xj - xi > 0 \\ 0\ xj - xi = 0 \\ -1\ xj - xi < 0 \end{cases} \tag{2}$$

xi and xj are the sample data values, n is the length of the analyzed data, and sign is the sign function.

The trend test statistic was as follows:

$$U_{MK} = \begin{cases} (\tau - 1)\Big/[Var(\tau)]^{\frac{1}{2}}\ \tau > 0 \\ 0\ \tau = 0 \\ (\tau + 1)\Big/[Var(\tau)]^{\frac{1}{2}}\ \tau < 0 \end{cases} \tag{3}$$

$$\mathrm{Var}(\tau) = \frac{n(n-1)(2n+5) - \sum_{i=1}^{m} t_i(t_i - 1)\ (2t_i + 5)}{18} \tag{4}$$

n is the number of samples, m is the number of repeated arrays in the sequence, and t_i is the number of repeated data in the i-th group of repeated arrays. When n >10, U tends to a standardized normal distribution. Assuming that the original series data have no trend, the significance level α is set to 0.05, and a two-sided trend test is used. If $|U_{MK}| \rangle U_{\alpha/2}$, we reject the original hypothesis, and the trend is significant; otherwise, we accept the original hypothesis, and the trend is not significant (Gocic and Trajkovic, 2013).

2.2.3. Geographic detector

The geographic detector is a model that detects spatial differentiation and its drivers. Using the factor detector and risk detector of the geographic detector, with 17 influencing factors as independent variables and SOS as the dependent variable, we explored the explanatory power of various factors on the SOS.

The factor detector detects the spatial differentiation of Y and the ability of a factor X to explain the spatial differentiation of attribute Y, which is measured by the q value (Wang et al., 2010, 2016). The expression is as follows:

$$\mathrm{q} = 1 - \frac{\sum_{h=1}^{L} N_h\sigma_h^2}{N\sigma^2} = 1 - \frac{SSW}{SST} \tag{5}$$

$$\mathrm{SSW} = \sum_{h=1}^{L} N_h\sigma_h^2 \tag{6}$$

$$\mathrm{SST} = \mathrm{N}\sigma^2 \tag{7}$$

h = 1, …, L is stratification, N_h is the number of units in layer h, N is the number of units in the whole region, σ_h^2 is the variance in layer h, σ^2 is the variance in the whole region, SSW is the sum of variance within layers, and SST is the total variance in the whole region.

The original data of the SOS and 17 influencing factors are raster data. We separately averaged these long-term series data pixel by pixel. All factors were set to the same coordinate system as the SOS and were resampled to a spatial resolution of 8 km by the nearest neighbor method. The SOS and influencing factors were converted into point data. One point contains one SOS and 17 influencing factors, which are average values over multiple years. We used classification methods such as natural breaks, equal intervals, and quantiles to discretize the influencing factors into 6 intervals, that is, L = 6. Table S1 shows the threshold value of influencing factors at each level. We can calculate the variance of the SOS in each subregion (σ_i^2) and the variance of the study region (σ^2) to obtain q. The term q varies in the range of [0,1], and the closer the q value is to 1, the more energetically X interprets Y, and conversely, the weaker it is.

A risk detector is used to identify favorable and unfavorable levels of environmental factors on the response variable. This is achieved by measuring the significance of differences between the two levels of environmental factors using t-tests. We used a risk detector to compare whether there was a significant difference in the SOS at different levels of influencing factors (Table S1) and to find the range of the influencing

factors corresponding to the maximum change in the SOS.

The *t*-test (Wang and Xu, 2017) was calculated as follows:

$$t_{\overline{y}_{h=1}-\overline{y}_{h=2}} = \frac{\overline{Y}_{h=1} - \overline{Y}_{h=2}}{\left[\frac{Var(\overline{Y}_{h=1})}{N_{h=1}} + \frac{Var(\overline{Y}_{h=2})}{N_{h=2}}\right]^{1/2}} \quad (8)$$

$\overline{Y}$, Var and N are the average, variance and the number of layers of the data Y, respectively. The original hypothesis indicates that there is no difference between layer 1 and layer 2.

2.2.4. Random forest regression model

Random forest is an ensemble learning method based on a nonparametric regression algorithm that is an extension of the decision tree and can solve the problems of overfitting and nonlinearity in general regression analysis. Decision tree is a commonly used method for classification and regression with a tree structure. Random forest is a combined classification model consisting of multiple decision tree models. There is no connection between trees. Each tree analyzes and votes on the results based on the input data and summarizes the results. The result with the most votes is the final output result (Machado et al., 2015). In this paper, we used the same projection coordinates for SOS and influencing factors and resampled them to the same resolution. SOS was used as the dependent variable, and 17 influencing factors were used as explanatory variables to construct a random forest regression model. We randomly selected 90 % of all sample points as the training set and 10 % as the test set. The training set was used to build the model, and the test set was used to score the performance of the model. After continuous optimization of the model, the final number of decision trees was set to 200. Based on random forest, we explored the driving factors affecting the differences in the spatial distribution of the SOS in the Northern Hemisphere and ranked the importance of the influence of each variable.

2.2.5. Multiple linear regression

To compare the relative importance among the environmental factors on the SOS, multiple linear regression showed the relationship between the SOS and influencing factors and quantitatively determined the influence degree of influencing factors on the interannual variation in the SOS. All data are raster data. The regression coefficient of each influencing factor was calculated from the pixel scale using a multiple linear regression model and standardized, and the factor with the largest absolute value of the standardized regression coefficient was taken as the most dominant factor affecting the SOS in the pixel.

2.2.6. Partial correlation analysis

To eliminate the influence of other environmental factors, the influence degree and direction of dominant factors on the SOS were examined. We used partial correlation analysis to determine the ability of dominant factors to influence the interannual variation in the SOS. The partial correlation coefficient between the influencing factors and SOS was tested by a *t*-test ($P < 0.05$).

3. Results

3.1. Detection of the variation of the SOS

Based on the Sen + Mann–Kendall method, the variation trend of the SOS in the Northern Hemisphere was obtained. Over the past 34 years, the average value of the SOS in the Northern Hemisphere showed an advancing trend. The trend in SOS advancement was more significant from 1982 to 1998, with the SOS advancing by 0.18 days/year ($P < 0.01$), while the SOS advanced by only 0.002 days/year ($P < 0.01$) from 1998 to 2015 (Fig. 1). At the pixel scale, 27.88 % of the pixels in the SOS in the Northern Hemisphere had a significant advancing or delaying trend ($P < 0.05$). The pixels showing a significant advancing trend

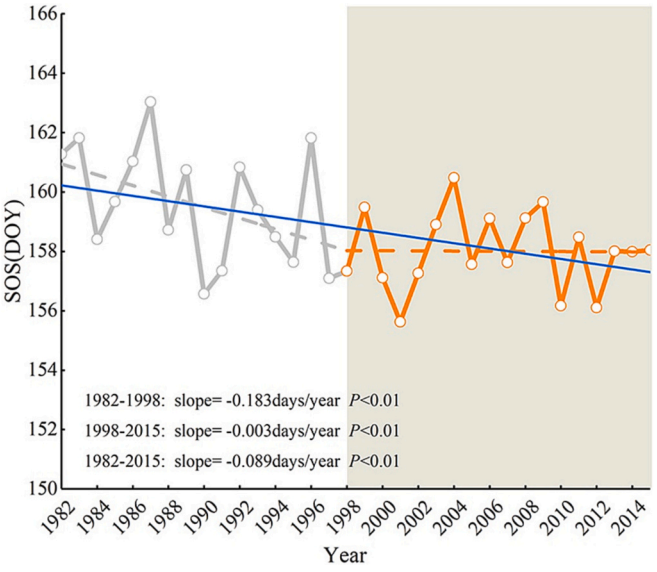

Fig. 1. Temporal trend in annual average values of SOS over the entire Northern Hemisphere from 1982 to 2015, 1982 to 1998 and 1998 to 2015.

accounted for 74.23 % of the pixels with a significant trend and were mainly distributed in Europe and Asia. The pixels showing a significant delaying trend accounted for 25.77 % of the pixels with a significant trend and were mainly distributed in North America. Among the pixels with significant changes, those with SOS trends between −1 and 1 days/year accounted for over 96 % of the pixels with significant trends (Fig. 2). Among them, the proportion of pixels with SOS trends between −0.5 and 0 days/year was 50.17 %; the proportion of pixels between −1 and −0.5 days/year was 22.25 %; the proportion of pixels between 0 and 0.5 days/year was 15.78 %; and the proportion of pixels between 0.5 and 1 days/year was 8.76 % (Fig. 2).

3.2. The dominant influencing factors of the SOS

3.2.1. Dominant factors of the SOS on the spatial scale

Based on geographic detector and random forest regression models, we explored the dominant drivers of the spatial differentiation of the SOS in the Northern Hemisphere. A total of 17 influencing factors were selected in this paper. Among them, longitude (LON), latitude (LAT) and elevation (DEM) were the geographic factors affecting the SOS; nighttime stable light (NTL), land cover (LC) and LST were the anthropogenic factors affecting the SOS; and NDVI was the vegetation factor affecting the SOS. In the CRU dataset, we selected the CLD, DTR, FRS, TMP, TMX, TMN, PET, PRE, VAP and WET as the climatic factors affecting the SOS.

Based on the results of the factor detector, the q-value quantified the extent to which influential factors explain the SOS in the Northern Hemisphere. The seven influencing factors of LST, TMX, TMP, FRS, LAT, TMN and VAP had the greatest impact on the SOS. The q-values were all above 0.4. In addition, 17 influencing factors all passed the 99 % confidence test. This suggests that these influencing factors play a decisive role in the SOS distribution (Fig. 3).

Based on the random forest regression model, we explored the importance proportions of 17 influencing factors on the distribution pattern of the SOS in the Northern Hemisphere. The LST, TMX, FRS, LAT, VAP, TMP, DTR, LC and NDVI were the top 9 influencing factors in terms of importance. Among them, the importance proportions of the LST and TMX were not <15 %, making these factors the dominant factors affecting the SOS (Fig. 3).

3.2.2. Dominant factors of the SOS on the time scale

The influencing factors consistent with the time length of SOS were

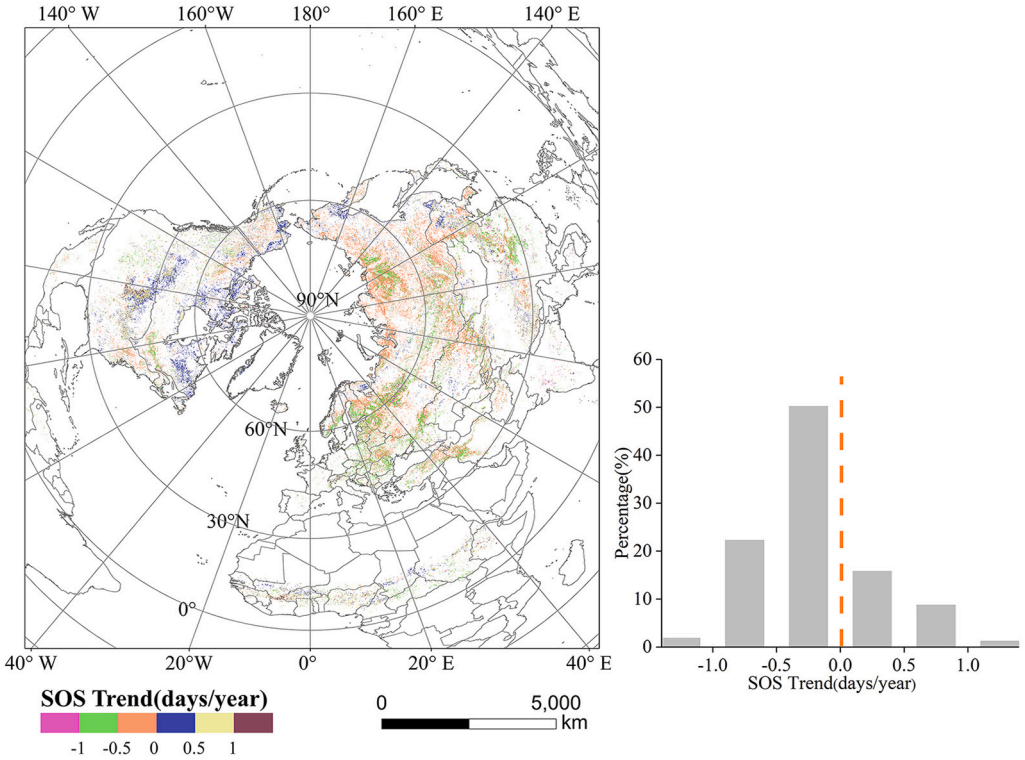

Fig. 2. Temporal and spatial trend (a) and percentage distribution (b) of the SOS in the Northern Hemisphere from 1982 to 2015 ($P < 0.05$).

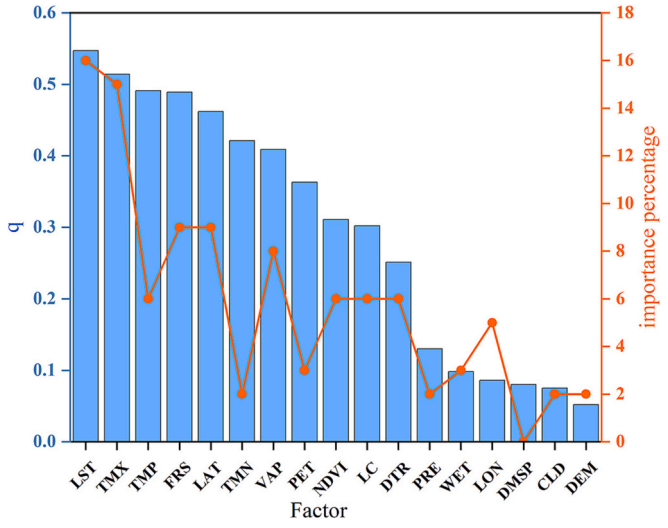

Fig. 3. The blue bar chart is the q-values of the SOS in the Northern Hemisphere under factor detection ($P < 0.01$), and the orange dot plot ranks the importance of the factors influencing the SOS (%) under the random forest regression model.

selected, namely, CLD, DTR, FRS, TMP, TMX, TMN, PET, PRE, VAP, WET and NDVI. The relative importance of the 11 influencing factors on the interannual variation in the SOS was obtained from the pixel scale using multiple linear regression. Fig. 4 shows the spatial distribution of the dominant factors. Overall, the multiple regression model concluded that temperature (TMP and TMX) explained 81 % of the interannual variation in the SOS in pixels, FRS explained 14 % of the interannual variation in the SOS in pixels, and humidity (VAP) explained 5 % of the interannual variation in the SOS in pixels.

Combining the results of the geographic detector and random forest regression model based on the spatial differentiation of the SOS on the spatial scale and the results of the multiple linear regression model based on the interannual variation in the SOS on the time scale, we found that the temperature (TMP and TMX). In addition, the spatial scale, including temperature-related LST and LAT, humidity (VAP), and frost frequency (FRS), were the dominant factors influencing the SOS variation in the Northern Hemisphere.

3.3. Impact characteristics of dominant factors on SOS

3.3.1. Impact of factors on the SOS on the spatial scale

The influence of the dominant factors on the SOS in the Northern Hemisphere was bidirectional, with the factors exhibiting both inhibitory and driving effects. With the increase in the LST, TMX and TMP, the SOS initially showed a trend of advance and then a trend of delay. There was a threshold of influence for temperature indicators. When the LST, TMX and TMP were above 20 °C, the SOS showed inhibition with increasing temperature. Overall, the FRS showed an inhibitory influence on the SOS. The SOS showed a delaying trend with increasing FRS. However, at the same time, an appropriate FRS may be beneficial to the occurrence of SOS. We found that the SOS started later when the FRS was very low. The variation trend of the SOS showed latitudinal divergence. At low latitudes, the SOS was positively correlated with latitude; at mid-latitudes, the SOS was negatively correlated with latitude; and at high latitudes, the SOS was positively correlated with latitude. When the VAP was 15 hPa, there were two aggregation centers of the SOS, approximately the 120th day and the 220th day. When the VAP was <15 hPa, the SOS showed an advancing trend toward the 120th day. When the VAP was >15 hPa, the SOS showed an advancing trend away from the 220th day (Fig. 5).

Based on the risk detection of the geographic detector, we used the natural interruption method to classify the LST, TMX, FRS, LAT, VAP and TMP into 6 grade intervals (Table S1). The temperature indicators (LST, TMX, and TMP) drove the SOS in intervals 1 to 5 and inhibited the SOS in interval 6. The driving interval for LST was [−22.6 °C, 20.7 °C], and the inhibition interval was (20.7 °C, 34.4 °C]. The driving interval

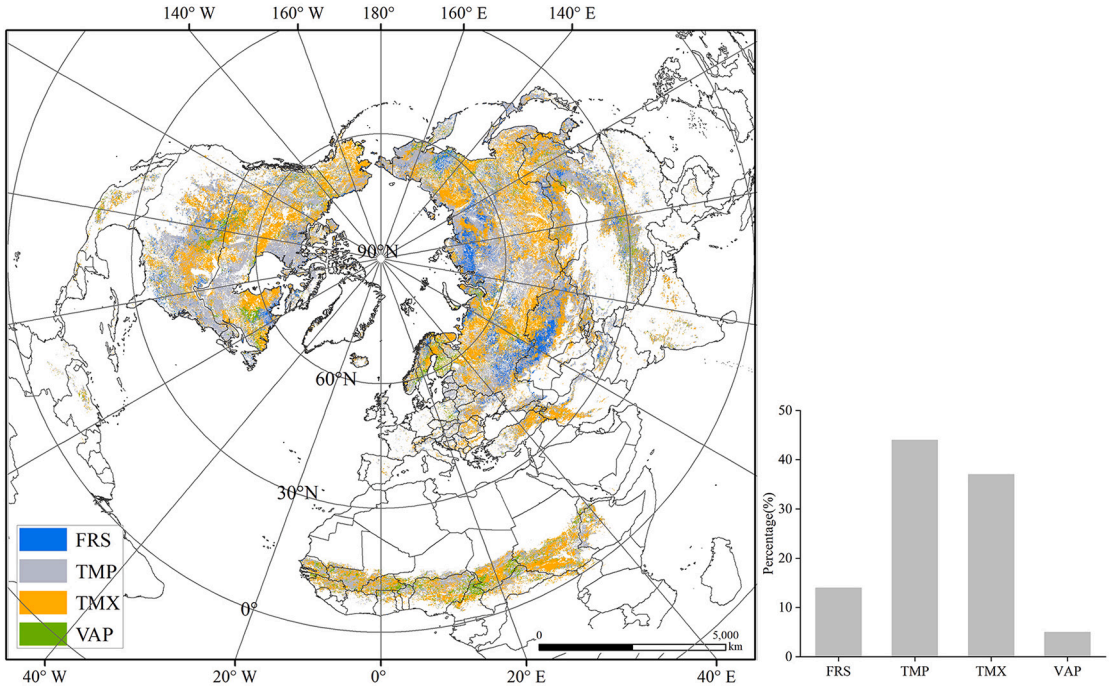

Fig. 4. The relative importance of influencing factors to the interannual variation in the SOS. The left shows the spatial distribution of the dominant factors, and the right shows the pixel proportion distribution of the dominant factors.

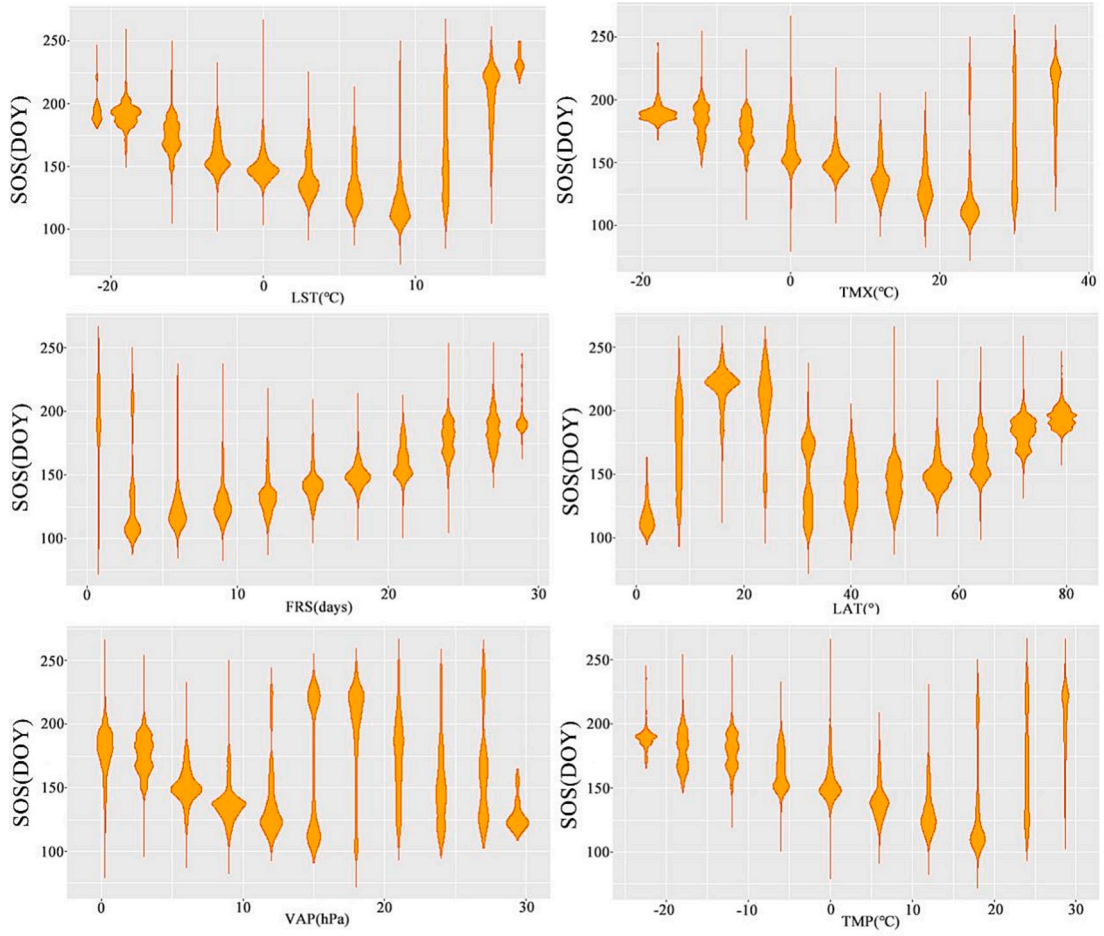

Fig. 5. Violin diagram of the relationship between dominant factors (LST, TMX, FRS, LAT, VAP, TMP) and the SOS. The continuous variables are shown in groups, where the group width of LST, TMX and TMP was 6, the group width of FRS and VAP was 3, and the group width of LAT was 8.

for TMX was [−20.7 °C, 24.7 °C], and the inhibition interval was (24.7 °C, 38 °C]. The driving interval for TMP was [−24 °C, 18.7 °C], and the inhibition interval was (18.7 °C, 30.3 °C]. When the FRS was in the interval from 2 to 6, the increase in the FRS inhibited the SOS with an inhibition interval of 4.89 days and 29.3 days. When the FRS was in interval 1 [0 days, 4.89 days], the average value of the SOS was the 181st day. When the FRS was low, the average value of the SOS was not the lowest, which means that a suitable FRS may be beneficial to the occurrence of SOS. When latitude was in the interval 3 to 6, the SOS showed a delayed trend with increasing latitude, and the inhibition intervals were between 27.5° and 82.2°. The latitude was in interval 1 [0.09°, 13.8°], and the average value of the SOS was on the 183rd day. The latitude was in interval 2 (13.8°, 27.5°], and the average value of the SOS was the 214th day. When the VAP was in the interval 1 to 4, the increase in the VAP drove the SOS with a driving interval of (0 hPa, 13.7 hPa]. When the VAP was in interval 5 (3.7 hPa, 19.4 hPa], the average value of the SOS was on the 182nd day. When the VAP was in interval 6 (19.4 hPa, 30.3 hPa], the average value of the SOS was the 169th day (Fig. 6).

Based on the risk detection of the geographic detector, we obtained the influence thresholds for all factors. We detected the characteristics of the SOS response to the dominant factors within the thresholds. By constructing a univariate linear regression equation between the SOS and dominant factors (LST, TMX, FRS, LAT, VAP, and TMP), we found that there was a strong relationship between the SOS and 6 dominant factors (Fig. S2). Temperature indicators (LST, TMX, TMP) all drove the SOS. When the LST was in the interval of [−22.6 °C, 20.7 °C], an increase in the LST by 1 °C advanced the SOS by 1.96 days. When the TMX was in the interval of [−20.7 °C, 24.7 °C], an increase in the TMX by 1 °C advanced the SOS by 1.95 days. When the TMP was in the interval of [−24 °C, 18.7 °C], an increase in the TMP by 1 °C advanced the SOS by 1.93 days. When the FRS was >4.89 days, an increase in the FRS inhibited the SOS. An increase in the FRS by 1 day delayed the SOS by 3.71 days. When the latitude was >27.5°, the SOS was positively correlated with latitude. An increase in latitude by 1° delayed the SOS by 1.34 days. When the VAP was <13.7 hPa, the VAP drove the SOS. An increase in the VAP by 1 hPa advanced the SOS by 6.82 days. There was a strong correlation between the SOS and 6 influencing factors (LST,

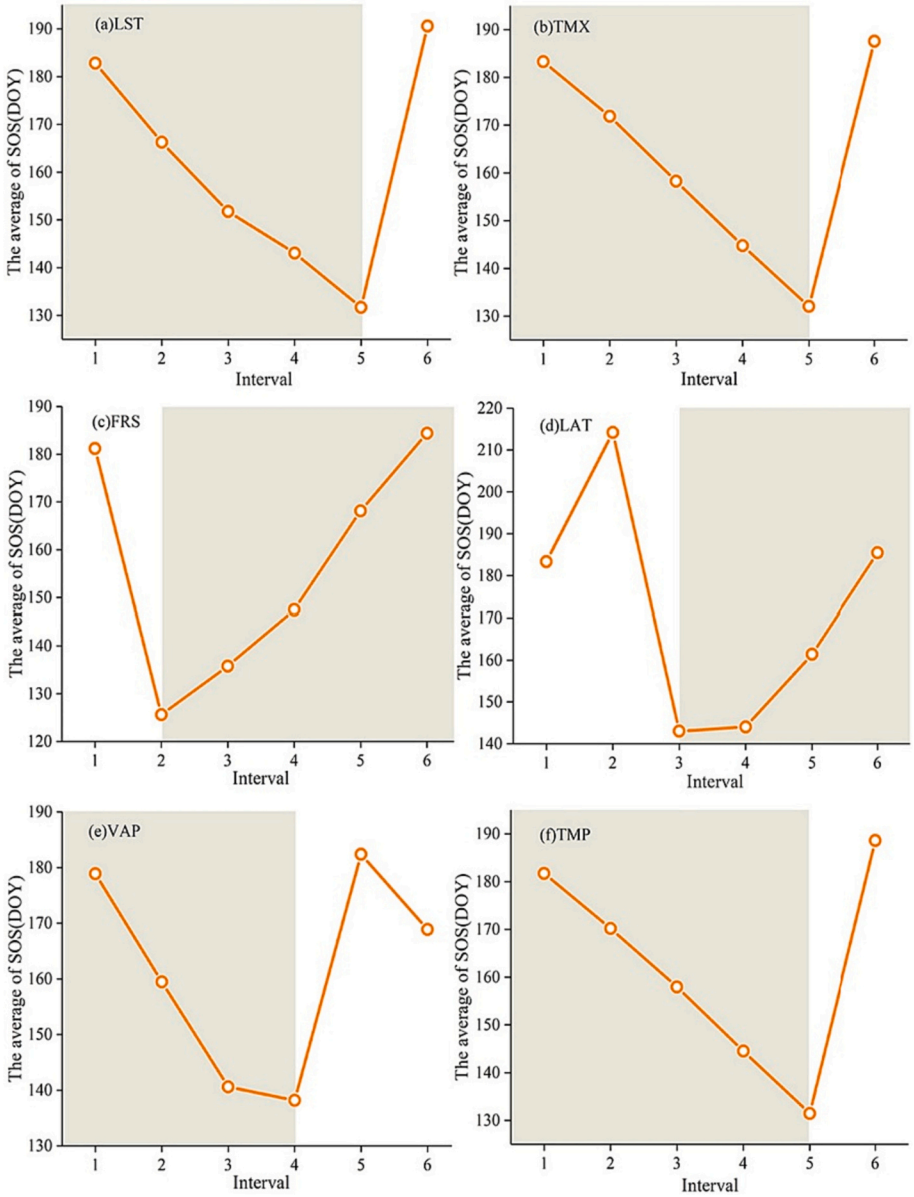

Fig. 6. The average value of the SOS in each interval for 6 dominant factors (LST, TMX, FRS, LAT, VAP, and TMP). The risk detector of the geographic detector divides the dominant factors into 6 intervals, and each interval has a threshold range.

TMX, FRS, LAT, VAP and TMP) ($R^2 > 0.4$, $P < 0.01$). The FRS and LST had the strongest correlations with SOS ($R^2 = 0.61$, $P < 0.01$) (Fig. S2).

3.3.2. Impact of factors on SOS on the time scale

FRS, TMP, TMX and VAP were the dominant factors affecting the interannual variation in the SOS. Using the partial correlation analysis method, we found that frost in 35.6 % of the pixels was positively correlated with the SOS, the increase in frost inhibited the SOS, 1 % of the pixels were negatively correlated with the SOS, and the increase in frost promoted the SOS. The influence of the temperature index on the SOS was different. A total of 19.7 % of the pixels indicated that the increase in TMX promoted the advance of the SOS, but 15.9 % of the pixels indicated that the increase in TMP led to the delay of the SOS. VAP can reflect the water conditions of the environment, and the results showed that the increase in VAP in 10.4 % of the pixels led to the delay of SOS, and the increase in VAP in 5.4 % of the pixels promoted the advance of the SOS (Fig. 7).

4. Discussion

4.1. Variation in the SOS

We found that the SOS significantly advanced in a majority of regions in Europe and Asia. In contrast, the SOS was significantly delayed in a majority of regions in North America (Fig. 2). These results were consistent with the research results of other scholars (Barichivich et al., 2013; Cohen et al., 2012; Wang et al., 2015; Zhao et al., 2015). Since the 1980s, the temperature in Europe has increased significantly, with extreme warm events in spring occurring more frequently (Crabbe et al., 2016). Strong anticyclonic conditions and warm air advection from the Atlantic Ocean have helped warm the surface of Europe (Luterbacher et al., 2007). This has created favorable temperature conditions for

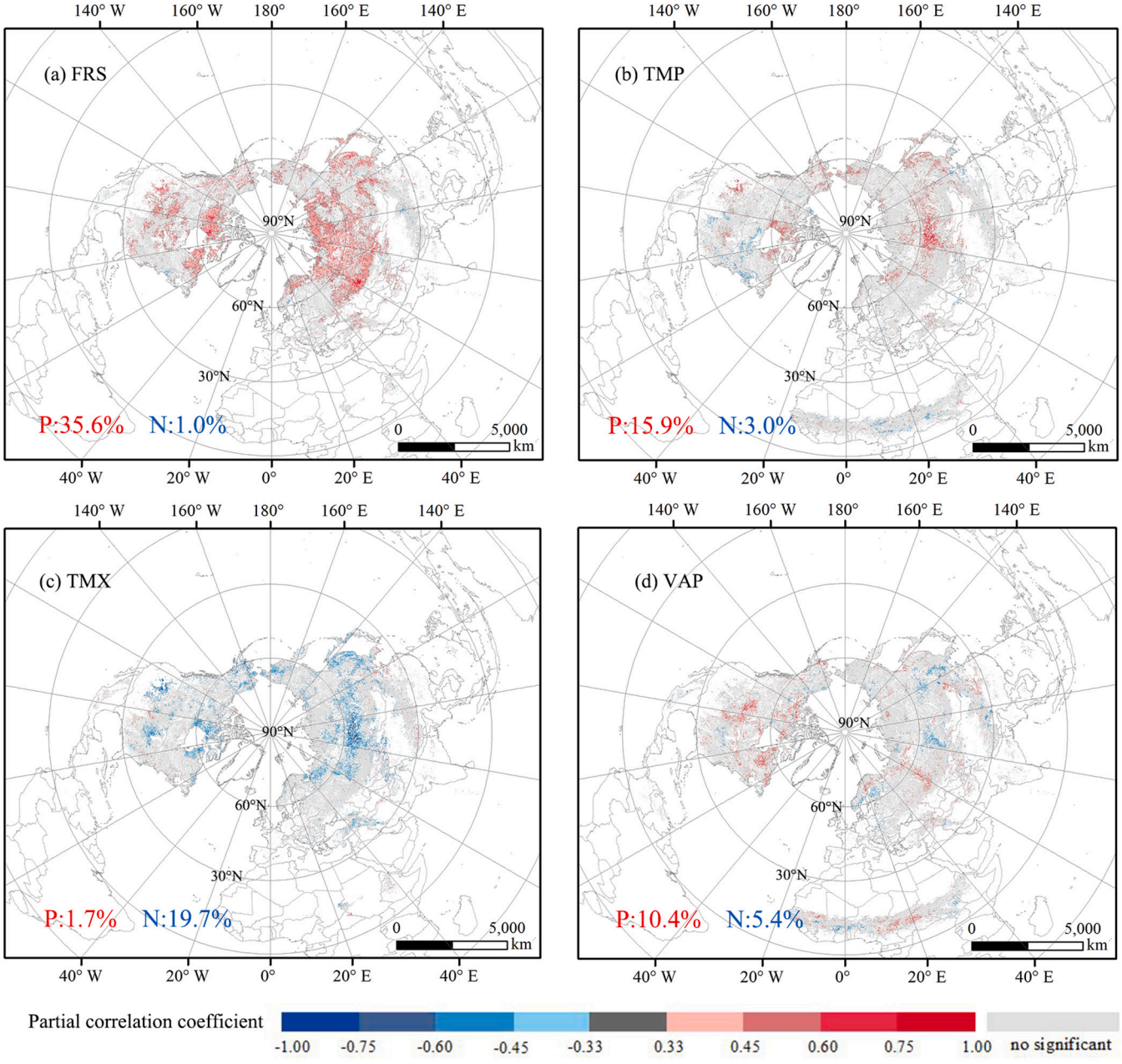

Fig. 7. (a) Partial correlation between the SOS and FRS. (b) Partial correlation between the SOS and TMP. (c) Partial correlation between the SOS and TMX. (d) Partial correlation between the SOS and VAP. The gray color in a, b, c and d represents a nonsignificant correlation. Significance was set at $P < 0.05$.

vegetation germination. The SOS was significantly delayed in most regions in North America. This is because the interannual spring temperature variability (STV) was higher in the North American region than in the European and Asian regions. Vegetation in high-STV regions has a higher demand for low temperatures. Under conditions with shorter winters, vegetation needs more heat to germinate. The proportion of heat demand was the highest in North America and the lowest in East Asia (Zohner et al., 2017). Therefore, in a warmer climate, rising temperatures may lead to a significant advance in the SOS in Asia. Due to the inability to meet the low-temperature requirements of vegetation in North America, the germination of North American vegetation was hindered. The average value of the SOS changed with different trends from 1982 to 2015. With 1998 as the breakpoint, the SOS advanced by trends of 0.18 days/year before 1998 and by 0.002 days/year after 1998 (Fig. 1). Previous studies have shown a hiatus in global warming between 1998 and 2012. The trend of the SOS advance slowed due to the slow rise in spring and annual average temperature. In addition, temperature change slowdowns during the warming hiatus were more common in North America than in Eurasia. Thus, the weakening of the SOS advancing trend during the warming hiatus was more prevalent in North America than in Eurasia (Wang et al., 2019b).

4.2. Influencing factors of the SOS

Frost frequency, temperature and humidity were the dominant drivers of interannual variability and spatial differentiation of the SOS in the Northern Hemisphere. The temperature index includes the TMX and TMP. In addition, the factors that determine the spatial differentiation of the SOS at the spatial scale also include LST and LAT. The humidity index corresponds to the VAP.

Temperature is an important factor influencing the variation in the SOS. Latitude is an indicator of geographical location, and it is essentially the decline of heat from the equator to the poles that causes the natural zone to show regular changes with latitude. Changes in SOS are highly dependent on changes in temperature, but SOS does not show a linear response to increasing temperature (Chuine et al., 2010). The direction and magnitude of change in the SOS with increasing temperature are not fixed. Two potential mechanisms may account for this phenomenon. On the one hand, vegetation is inconsistent with calorie needs during different growth stages. Vegetation needs a certain amount of low temperatures to break the dormant period, and a mild winter leads to insufficient low temperature accumulation, which delays the leaf-spreading time (Song et al., 2020). However, a rise in spring temperature accelerates the heat accumulation of vegetation and accelerates the growth of vegetation in spring (Yu et al., 2010). On the other hand, temperature and photoperiod combine to regulate vegetation leaf spreading time (Chew et al., 2012). With the increase in temperature, vegetation can carry out photosynthesis better, which is beneficial to vegetation carbon fixation and heat accumulation (Piao et al., 2015). A longer photoperiod makes up for the lack of the accumulation of cold temperatures during warm winters, facilitating the release of vegetation from dormancy (Way and Montgomery, 2015). The cold reserve of vegetation in warm winters is insufficient, which increases the demand for heat. It takes a long enough photoperiod for vegetation to sprout. Insufficient sunshine increases the demand for calories for vegetation. These factors limit the advancement of the SOS and reduce the sensitivity of vegetation to climate warming. (Fu et al., 2019). In short, the combination of photoperiod and temperature regulates the ratio of cold to heat requirements of vegetation to produce leaves at the optimum time and avoid damage from frost.

Frost damage to vegetation is very serious. The timing of vegetation germination and leaf spreading is directly or indirectly controlled by frost (Wang et al., 2019a). The severity of frost damage to vegetation is related to when it occurs. When frost occurs in early spring, it is not easy to capture heat and trigger spring phenology. When frost occurs in late spring, its damage to vegetation can be divided into two stages. In the first stage, the temperature rises in early spring, and the vegetation germinates earlier. In the second stage, when the temperature drops below the threshold of the appropriate survival of vegetation, the cold resistance of vegetation is weak, and the sudden temperature drop will cause serious damage to the young growing tissues and organs of vegetation (Gu et al., 2008). Some scholars have discussed climate warming and frosts occurring in late spring that will cause superposition damage to vegetation in related studies (Koźmiński et al., 2021). In addition, frost also interacts with other environmental factors. Higher atmospheric CO_2 concentrations reduce the tolerance of vegetation to low temperatures, making vegetation more vulnerable to cold conditions (Beerling et al., 2001). Climate warming also increases the likelihood of environmental drought, which is not conducive to vegetation regeneration and recovery after frost (Gu et al., 2008). Therefore, under the current environment of rapid global warming and high CO_2 concentrations, the combination of frost and other environmental factors is likely to result in greater vegetation damage and to become the main factor affecting the SOS. In addition, the results of this paper suggest that appropriately timed frost may also be beneficial to the occurrence of the SOS: because the recovery of vegetation in spring requires a certain low temperature, an appropriately timed frost event may be beneficial to the accumulation of low temperatures.

The SOS is also greatly affected by the VAP. To a certain extent, the VAP can represent the water vapor content of the atmosphere, which affects the transpiration of vegetation. The vapor pressure deficit (VPD) can be calculated from the VAP, which is negatively correlated with the VAP (Cai et al., 2019). The VPD is often used to assess the temperature and humidity levels of the atmosphere (Zhou et al., 2019). Previous studies have shown that climate warming leads to aggravation of the saturated water VPD. The high saturated water VPD not only affects vegetation physiology but also leads to an increase in the water loss rate of moist soils, which in turn leads to drying and heating of the land surface, resulting in frequent and severe drought events and vegetation water stress (Xiao et al., 2020). This in turn means that a low VAP exerts an inhibitory effect on the SOS by limiting the moisture available to vegetation.

4.3. Impact characteristics of dominant factors on SOS

Our results showed that there are thresholds for all drivers. Appropriate frost is conducive to low temperature accumulation of vegetation, but excessive frost will cause irreversible damage to vegetation. An increase in the temperature indicators (LST, TMP, TMX) promoted the advancement of the SOS. Existing studies have shown that there are differences in the sensitivity of the SOS to the TMX and TMN and that an increase in TMX is more likely to trigger the SOS (Fu et al., 2016; Piao et al., 2015). Our results also showed that the SOS was more significantly affected by the TMX. The latitude threshold was 27.5°N. Above 27.5°N, the SOS was positively correlated with latitude. Previous studies have shown that the latitudinal pattern of temporal changes in the SOS under climate warming in the range of 30°N to 75°N can be explained by the latitude dependence of the sensitivity of vegetation to preseason temperature. The SOS was more sensitive to temperature at lower latitudes and started earlier at lower latitudes (Shen et al., 2015). Our results further expanded the latitude threshold interval. The TMP has errors and limitations in explaining the SOS variation. (Piao et al., 2015) proposed that SOS was triggered by TMX rather than TMN and TMP, and (Wu et al., 2018) proposed that the effects of TMX and TMN on phenology were opposite, and the direct use of TMP would reduce the ability of temperature to affect vegetation. Fig. 7 illustrates that TMX can describe the effect of temperature on SOS more accurately than TMP. In addition, the synergistic effect of temperature and VAP can also cause the SOS to change in an advanced direction under the condition of low VAP, as shown in Fig. 7. On the one hand, because the temperature rises, vegetation germinates prematurely and increases the demand for water. At this time, insufficient precipitation will lead to environmental

drought and then form a positive correlation between the SOS and VAP (Zhang et al., 2021). On the other hand, the increase in VAP in the threshold range could reduce the water stress of vegetation and drive the SOS. However, an excessive VAP means that the atmosphere is too humid, which results in soil temperatures that are too cold and require more heat to trigger SOS (Fu et al., 2014).

The SOS showing significantly advanced and significantly delayed regions in 1982–2015 are shown in Fig. S3. In regions where the SOS significantly advanced, the SOS was mainly controlled by frost frequency, temperature factors (TMP, TMN, TMX) and humidity factors (PET, VAP, WET). Reduced frost, increased temperature and reduced water stress promoted SOS advancement (Fig. S4). However, it is worth noting that the regions where the SOS was significantly delayed in this research also showed increased temperature, decreased frost frequency and decreased water stress (Fig. S5). The regions with significantly delayed SOS were mainly located in North America and were dominated by grassland and farmland vegetation types (Fig. S6). The timing of crop leaf development is determined more by human factors than by climate change. Therefore, despite warming conditions, vegetation may also show late leaf expansion. In addition, previous studies have shown that the effects of warming and increased precipitation on the SOS are not necessarily promoting effects. On the one hand, warming in winter is not conducive to low temperature accumulation in vegetation (Song et al., 2020). On the other hand, increased precipitation increases the moisture in the soil environment of vegetation, which may cause the soil temperature to be lower than expected and therefore require more heat to trigger the SOS (Fu et al., 2014). Another explanation is that the beginning of the SOS requires a certain threshold of solar radiation, and rainy days are not conducive to the capture of solar radiation energy (Fu et al., 2014). Therefore, in regions dominated by grassland vegetation types, the SOS showed a delaying trend under a warmer environment with less water stress, probably reflecting the inhibitory effect of temperature and humidity factors. In the future, more research should be done on the factors influencing the delayed SOS in the Northern Hemisphere.

5. Conclusions

We used the GIMMS3g NDVI dataset to extract the SOS based on various phenological extraction models. We found that from 1982 to 2015, the SOS in some regions of Europe and Asia showed an advancing trend, and the trend was mainly concentrated between 0 and 1 days in advance every year. The SOS in some regions of North America showed a delayed trend, and the vegetation types in the delayed regions were mainly grassland and farmland. Combining the results of the geographic detector model, the random forest regression model and multiple linear regression, the dominant drivers of the SOS in the Northern Hemisphere were frost frequency, temperature and humidity. An increase in frost inhibited the SOS. A temperature increase advanced the SOS. Humidity factors affected the SOS by affecting the water stress environment of vegetation and by acting synergistically with temperature indicators. Each main driving factor had a certain influence threshold. Outside the threshold ranges, the response relationships between the SOS and the influencing factors were relatively weak.

CRediT authorship contribution statement

All authors contributed to the design and the accomplishment of this work. **Haihua Chen:** Conceptualization, Methodology, Software, Formal analysis, Writing - original draft. **Jianjun Zhao**, **Hongyan Zhang:** conceptualization, methodology, writing - review & editing, supervision, validation. **Zhengxiang Zhang**, **Xiaoyi Guo**, **Meiyu Wang:** Methodology, Software, Data curation. **Jianjun Zhao:** conceptualization, methodology.

Declaration of competing interest

The authors declare that they have no known competing financial interests or personal relationships that could have appeared to influence the work reported in this paper.

Data availability

Data will be made available on request.

Acknowledgements

This work was financially supported by the National Natural Science Foundation of China (Grant Nos. 42171321 and 41871330), the Basic Construction Funds (innovation capacity building) for the budget of Jilin Province in 2023 (2023C030-1) and the National Key Research and Development Program of China (No. 2020YFA0714100).

Appendix A. Supplementary data

Supplementary data to this article can be found online at https://doi.org/10.1016/j.scitotenv.2023.166607.

References

Barichivich, J., Briffa, K.R., Myneni, R.B., Osborn, T.J., Melvin, T.M., Ciais, P., Piao, S., Tucker, C., 2013. Large-scale variations in the vegetation growing season and annual cycle of atmospheric CO $_2$ at high northern latitudes from 1950 to 2011. Glob. Change Biol. 19, 3167–3183. https://doi.org/10.1111/gcb.12283.

Beck, P.S.A., Atzberger, C., Høgda, K.A., Johansen, B., Skidmore, A.K., 2006. Improved monitoring of vegetation dynamics at very high latitudes: a new method using MODIS NDVI. Remote Sens. Environ. 100, 321–334. https://doi.org/10.1016/j.rse.2005.10.021.

Beerling, D.J., Terry, A.C., Mitchell, P.L., Callaghan, T.V., Gwynn-Jones, D., Lee, J.A., 2001. Time to chill: effects of simulated global change on leaf ice nucleation temperatures of subarctic vegetation. Am. J. Bot. 88, 628–633. https://doi.org/10.2307/2657062.

Cai, Y., Guan, K., Lobell, D., Potgieter, A.B., Wang, S., Peng, J., Xu, T., Asseng, S., Zhang, Y., You, L., Peng, B., 2019. Integrating satellite and climate data to predict wheat yield in Australia using machine learning approaches. Agric. For. Meteorol. 274, 144–159. https://doi.org/10.1016/j.agrformet.2019.03.010.

Chew, Y.H., Wilczek, A.M., Williams, M., Welch, S.M., Schmitt, J., Halliday, K.J., 2012. An augmented Arabidopsis phenology model reveals seasonal temperature control of flowering time. New Phytol. 194, 654–665. https://doi.org/10.1111/j.1469-8137.2012.04069.x.

Chuine, I., Morin, X., Bugmann, H., 2010. Warming, photoperiods, and tree phenology. Science 329, 277–278. https://doi.org/10.1126/science.329.5989.276-a.

Cohen, J.L., Furtado, J.C., Barlow, M., Alexeev, V.A., Cherry, J.E., 2012. Asymmetric seasonal temperature trends: seasonal trends. Geophys. Res. Lett. 39, n/a-n/a. https://doi.org/10.1029/2011GL050582.

Crabbe, R.A., Dash, J., Rodriguez-Galiano, V.F., Janous, D., Pavelka, M., Marek, M.V., 2016. Extreme warm temperatures alter forest phenology and productivity in Europe. Sci. Total Environ. 563–564, 486–495. https://doi.org/10.1016/j.scitotenv.2016.04.124.

Craven, P., Wahba, G., 1979. Smoothing noisy data with spline functions. Numer. Math. 21, 377–403.

De Barba, D., Rossi, S., Deslauriers, A., Morin, H., 2016. Effects of soil warming and nitrogen foliar applications on bud burst of black spruce. Trees 30, 87–97. https://doi.org/10.1007/s00468-015-1152-0.

Delbart, N., Kergoat, L., Le Toan, T., Lhermitte, J., Picard, G., 2005. Determination of phenological dates in boreal regions using normalized difference water index. Remote Sens. Environ. 97, 26–38. https://doi.org/10.1016/j.rse.2005.03.011.

Deng, G., Zhang, H., Guo, X., Shan, Y., Ying, H., Rihan, W., Li, H., Han, Y., 2019. Asymmetric effects of daytime and nighttime warming on boreal forest spring phenology. Remote Sens. 11, 1651. https://doi.org/10.3390/rs11141651.

Elmore, A.J., Guinn, S.M., Minsley, B.J., Richardson, A.D., 2012. Landscape controls on the timing of spring, autumn, and growing season length in mid-Atlantic forests. Glob. Change Biol. 18, 656–674. https://doi.org/10.1111/j.1365-2486.2011.02521.x.

Fan, L., Zhao, J., Wang, Y., Ren, Z., Zhang, H., Guo, X., 2019. Assessment of night-time lighting for global terrestrial protected and wilderness areas. Remote Sens. 11, 2699. https://doi.org/10.3390/rs11222699.

Farlie, D.J.G., Kendall, M.G., 1971. Rank Correlation Methods.

Fischer, A., 1994. A model for the seasonal variations of vegetation indices in coarse resolution data and its inversion to extract crop parameters. Remote Sens. Environ. 48, 220–230. https://doi.org/10.1016/0034-4257(94)90143-0.

Friedman, J.H., Roosen, C.B., 1995. An introduction to multivariate adaptive regression splines. Stat. Methods Med. Res. 4, 197–217. https://doi.org/10.1177/096228029500400303.

Fu, Y.H., Piao, S., Zhao, H., Jeong, S.-J., Wang, X., Vitasse, Y., Ciais, P., Janssens, I.A., 2014. Unexpected role of winter precipitation in determining heat requirement for spring vegetation green-up at northern middle and high latitudes. Glob. Change Biol. 20, 3743–3755. https://doi.org/10.1111/gcb.12610.

Fu, Y.H., Liu, Y., De Boeck, H.J., Menzel, A., Nijs, I., Peaucelle, M., Peñuelas, J., Piao, S., Janssens, I.A., 2016. Three times greater weight of daytime than of night-time temperature on leaf unfolding phenology in temperate trees. New Phytol. 212, 590–597. https://doi.org/10.1111/nph.14073.

Fu, Y.H., Zhang, X., Piao, S., Hao, F., Geng, X., Vitasse, Y., Zohner, C., Peñuelas, J., Janssens, I.A., 2019. Daylength helps temperate deciduous trees to leaf-out at the optimal time. Glob. Change Biol. 25, 2410–2418. https://doi.org/10.1111/gcb.14633.

Fu, Y., Li, X., Zhou, X., Geng, X., Guo, Y., Zhang, Y., 2020. Progress in plant phenology modeling under global climate change. Sci. China Earth Sci. 63, 1237–1247. https://doi.org/10.1007/s11430-019-9622-2.

Gocic, M., Trajkovic, S., 2013. Analysis of changes in meteorological variables using Mann-Kendall and Sen's slope estimator statistical tests in Serbia. Glob. Planet. Chang. 100, 172–182. https://doi.org/10.1016/j.gloplacha.2012.10.014.

Gu, L., Hanson, P.J., Post, W.M., Kaiser, D.P., Yang, B., Nemani, R., Pallardy, S.G., Meyers, T., 2008. The 2007 eastern US spring freeze: increased cold damage in a warming world? BioScience 58, 253–262. https://doi.org/10.1641/B580311.

IPCC, 2018. IPCC's Special Report on Global Warming of 1.5 °C.

Jeong, S.-J., Ho, C.-H., Gim, H.-J., Brown, M.E., 2011. Phenology shifts at start vs. end of growing season in temperate vegetation over the Northern Hemisphere for the period 1982–2008: phenology shifts at start vs. end of growing season. Glob. Chang. Biol. 17, 2385–2399. https://doi.org/10.1111/j.1365-2486.2011.02397.x.

Jonsson, P., Eklundh, L., 2002. Seasonality extraction by function fitting to time-series of satellite sensor data. IEEE Trans. Geosci. Remote Sensing 40, 1824–1832. https://doi.org/10.1109/TGRS.2002.802519.

Keenan, T.F., Gray, J., Friedl, M.A., Toomey, M., Bohrer, G., Hollinger, D.Y., Munger, J. W., O'Keefe, J., Schmid, H.P., Wing, I.S., Yang, B., Richardson, A.D., 2014. Net carbon uptake has increased through warming-induced changes in temperate forest phenology. Nat. Clim. Change 4, 598–604. https://doi.org/10.1038/nclimate2253.

Körner, C., Basler, D., 2010. Phenology under global warming. Science 327, 1461–1462. https://doi.org/10.1126/science.1186473.

Koźmiński, C., Nidzgorska-Lencewicz, J., Mąkosza, A., Michalska, B., 2021. Ground frosts in Poland in the growing season. Agriculture 11, 573. https://doi.org/10.3390/agriculture11070573.

Luterbacher, J., Liniger, M.A., Menzel, A., Estrella, N., Della-Marta, P.M., Pfister, C., Rutishauser, T., Xoplaki, E., 2007. Exceptional European warmth of autumn 2006 and winter 2007: historical context, the underlying dynamics, and its phenological impacts. Geophys. Res. Lett. 34, L12704. https://doi.org/10.1029/2007GL029951.

Machado, G., Mendoza, M.R., Corbellini, L.G., 2015. What variables are important in predicting bovine viral diarrhea virus? A random forest approach. Vet. Res. 46, 85. https://doi.org/10.1186/s13567-015-0219-7.

Mann, H.B., 1945. Nonparametric tests against trend. Econometrica 13, 245. https://doi.org/10.2307/1907187.

Meng, F., Huang, L., Chen, A., Zhang, Y., Piao, S., 2021. Spring and autumn phenology across the Tibetan Plateau inferred from normalized difference vegetation index and solar-induced chlorophyll fluorescence. Big Earth Data 5, 182–200. https://doi.org/10.1080/20964471.2021.1920661.

Peñuelas, J., Rutishauser, T., Filella, I., 2009. Phenology feedbacks on climate change. Science 324, 887–888. https://doi.org/10.1126/science.1173004.

Piao, S., Fang, J., Zhou, L., Ciais, P., Zhu, B., 2006. Variations in satellite-derived phenology in China's temperate vegetation: satellite-derived phenology in China. Glob. Chang. Biol. 12, 672–685. https://doi.org/10.1111/j.1365-2486.2006.01123.x.

Piao, S., Ciais, P., Friedlingstein, P., Peylin, P., Reichstein, M., Luyssaert, S., Margolis, H., Fang, J., Barr, A., Chen, A., Grelle, A., Hollinger, D.Y., Laurila, T., Lindroth, A., Richardson, A.D., Vesala, T., 2008. Net carbon dioxide losses of northern ecosystems in response to autumn warming. Nature 451, 49–52. https://doi.org/10.1038/nature06444.

Piao, S., Tan, J., Chen, A., Fu, Y.H., Ciais, P., Liu, Q., Janssens, I.A., Vicca, S., Zeng, Z., Jeong, S.-J., Li, Y., Myneni, R.B., Peng, S., Shen, M., Peñuelas, J., 2015. Leaf onset in the northern hemisphere triggered by daytime temperature. Nat. Commun. 6, 6911. https://doi.org/10.1038/ncomms7911.

Piao, S., Liu, Q., Chen, A., Janssens, I.A., Fu, Y., Dai, J., Liu, L., Lian, X., Shen, M., Zhu, X., 2019. Plant phenology and global climate change: current progresses and challenges. Glob. Change Biol. 25, 1922–1940. https://doi.org/10.1111/gcb.14619.

Richardson, A.D., Andy Black, T., Ciais, P., Delbart, N., Friedl, M.A., Gobron, N., Hollinger, D.Y., Kutsch, W.L., Longdoz, B., Luyssaert, S., Migliavacca, M., Montagnani, L., William Munger, J., Moors, E., Piao, S., Rebmann, C., Reichstein, M., Saigusa, N., Tomelleri, E., Vargas, R., Varlagin, A., 2010. Influence of spring and autumn phenological transitions on forest ecosystem productivity. Phil. Trans. R. Soc. B 365, 3227–3246. https://doi.org/10.1098/rstb.2010.0102.

Roerink, G.J., Menenti, M., Verhoef, W., 2000. Reconstructing cloudfree NDVI composites using Fourier analysis of time series. Int. J. Remote Sens. 21, 1911–1917. https://doi.org/10.1080/014311600209814.

Savitzky, Abraham, Golay, M.J.E., 1964. Smoothing and differentiation of data by simplified least squares procedures. Anal. Chem. 36, 1627–1639. https://doi.org/10.1021/ac60214a047.

Shen, M., Zhang, G., Cong, N., Wang, S., Kong, W., Piao, S., 2014. Increasing altitudinal gradient of spring vegetation phenology during the last decade on the Qinghai–Tibetan Plateau. Agric. For. Meteorol. 189–190, 71–80. https://doi.org/10.1016/j.agrformet.2014.01.003.

Shen, M., Cong, N., Cao, R., 2015. Temperature sensitivity as an explanation of the latitudinal pattern of green-up date trend in Northern Hemisphere vegetation during 1982–2008: changes in latitudinal pattern of green-up date. Int. J. Climatol. 35, 3707–3712. https://doi.org/10.1002/joc.4227.

Song, Z., Song, X., Pan, Y., Dai, K., Shou, J., Chen, Q., Huang, J., Tang, X., Huang, Z., Du, Y., 2020. Effects of winter chilling and photoperiod on leaf-out and flowering in a subtropical evergreen broadleaved forest in China. For. Ecol. Manag. 458, 117766 https://doi.org/10.1016/j.foreco.2019.117766.

Studer, S., Stöckli, R., Appenzeller, C., Vidale, P.L., 2007. A comparative study of satellite and ground-based phenology. Int. J. Biometeorol. 51, 405–414. https://doi.org/10.1007/s00484-006-0080-5.

Tao, Z., Wang, H., Liu, Y., Xu, Y., Dai, J., 2017. Phenological response of different vegetation types to temperature and precipitation variations in northern China during 1982–2012. Int. J. Remote Sens. 38, 3236–3252. https://doi.org/10.1080/01431161.2017.1292070.

Wang, J., Xu, C.-D., 2017. Geodetector: principle and prospective. Acta Geograph. Sin. 72, 116–134. https://doi.org/10.11821/dlxb201701010.

Wang, J., Li, X., Christakos, G., Liao, Y., Zhang, T., Gu, X., Zheng, X., 2010. Geographical detectors-based health risk assessment and its application in the neural tube defects study of the Heshun Region, China. Int. J. Geogr. Inf. Sci. 24, 107–127. https://doi.org/10.1080/13658810802443457.

Wang, X., Piao, S., Xu, X., Ciais, P., MacBean, N., Myneni, R.B., Li, L., 2015. Has the advancing onset of spring vegetation green-up slowed down or changed abruptly over the last three decades?: 30-year change of spring vegetation phenology. Glob. Ecol. Biogeogr. 24, 621–631. https://doi.org/10.1111/geb.12289.

Wang, J.-F., Zhang, T.-L., Fu, B.-J., 2016. A measure of spatial stratified heterogeneity. Ecol. Indic. 67, 250–256. https://doi.org/10.1016/j.ecolind.2016.02.052.

Wang, Y., Case, B., Rossi, S., Dawadi, B., Liang, E., Ellison, A.M., 2019a. Frost controls spring phenology of juvenile Smith fir along elevational gradients on the southeastern Tibetan Plateau. Int. J. Biometeorol. 63, 963–972. https://doi.org/10.1007/s00484-019-01710-4.

Wang, X., Xiao, J., Li, X., Cheng, G., Ma, M., Zhu, G., Altaf Arain, M., Andrew Black, T., Jassal, R.S., 2019b. No trends in spring and autumn phenology during the global warming hiatus. Nat. Commun. 10, 2389. https://doi.org/10.1038/s41467-019-10235-8.

Way, D.A., Montgomery, R.A., 2015. Photoperiod constraints on tree phenology, performance and migration in a warming world. Plant Cell Environ. 38, 1725–1736. https://doi.org/10.1111/pce.12431.

White, M.A., Thornton, P.E., Running, S.W., 1997. A continental phenology model for monitoring vegetation responses to interannual climatic variability. Glob. Biogeochem. Cycles 11, 217–234. https://doi.org/10.1029/97GB00330.

Wu, C., Wang, X., Wang, H., Ciais, P., Peñuelas, J., Myneni, R.B., Desai, A.R., Gough, C. M., Gonsamo, A., Black, A.T., Jassal, R.S., Ju, W., Yuan, W., Fu, Y., Shen, M., Li, S., Liu, R., Chen, J.M., Ge, Q., 2018. Contrasting responses of autumn-leaf senescence to daytime and night-time warming. Nat. Clim. Change 8, 1092–1096. https://doi.org/10.1038/s41558-018-0346-z.

Xiao, M., Yu, Z., Kong, D., Gu, X., Mammarella, I., Montagnani, L., Arain, M.A., Merbold, L., Magliulo, V., Lohila, A., Buchmann, N., Wolf, S., Gharun, M., Hörtnagl, L., Beringer, J., Gioli, B., 2020. Stomatal response to decreased relative humidity constrains the acceleration of terrestrial evapotranspiration. Environ. Res. Lett. 15, 094066 https://doi.org/10.1088/1748-9326/ab9967.

Yu, H., Luedeling, E., Xu, J., 2010. Winter and spring warming result in delayed spring phenology on the Tibetan Plateau. Proc. Natl. Acad. Sci. U. S. A. 107, 22151–22156. https://doi.org/10.1073/pnas.1012490107.

Zhang, X., Friedl, M.A., Schaaf, C.B., Strahler, A.H., Hodges, J.C.F., Gao, F., Reed, B.C., Huete, A., 2003. Monitoring vegetation phenology using MODIS. Remote Sens. Environ. 84, 471–475. https://doi.org/10.1016/S0034-4257(02)00135-9.

Zhang, J., Zhao, J., Wang, Y., Zhang, H., Zhang, Z., Guo, X., 2020. Comparison of land surface phenology in the Northern Hemisphere based on AVHRR GIMMS3g and MODIS datasets. ISPRS J. Photogramm. Remote Sens. 169, 1–16.

Zhang, W., Li, Y., Wu, X., Chen, Y., Chen, A., Schwalm, C.R., Kimball, J.S., 2021. Divergent response of vegetation growth to soil water availability in dry and wet periods over Central Asia. J. Geophys. Res. Biogeosci. 126 https://doi.org/10.1029/2020JG005912.

Zhao, J., Zhang, H., Zhang, Z., Guo, X., Li, X., Chen, C., 2015. Spatial and temporal changes in vegetation phenology at middle and high latitudes of the Northern Hemisphere over the past three decades. Remote Sens. 7, 10973–10995.

Zhou, S., Zhang, Y., Park Williams, A., Gentine, P., 2019. Projected increases in intensity, frequency, and terrestrial carbon costs of compound drought and aridity events. Sci. Adv. 5, eaau5740. https://doi.org/10.1126/sciadv.aau5740.

Zohner, C.M., Benito, B.M., Fridley, J.D., Svenning, J.-C., Renner, S.S., 2017. Spring predictability explains different leaf-out strategies in the woody floras of North America, Europe and East Asia. Ecol. Lett. 20, 452–460. https://doi.org/10.1111/ele.12746.